A THREE-DIMENSIONAL STUDY OF NUCLEAR FUEL ROD BEHAVIOR DURING STARTUP

S. LEVY, J. P. D. WILKINSON

Corporate Research and Development,
General Electric Company, Schenectady, New York 12345, U.S.A.

SUMMARY

A three-dimensional finite element study is made of the behavior of cylindrical uranium dioxide fuel pellets during startup. The finite element code uses an 8-noded box element of arbitrary shape to build up the stiffness and stress characteristics by Gaussian integration. Each box has 33 degrees of freedom: 24 corresponding to the 3 motions at each of the 8 nodes; and 9 internally eliminated to minimize strain energy. The 9 internal degrees of freedom are highly effective in eliminating shear error, and thus permitting far fewer elements than are required when tetrahedron elements are used. The element uses an isoparametric approach, so that the box can have 8 arbitrarily positioned nodes. So long as the thermal expansions of the fuel rod can be described by a linear variation in the element, the code takes highly accurate account of it.

Plasticity is accounted for by the secant modulus approach. Friction between the pellet and the cladding can be introduced by springs between the relevant finite elements in each area. A new and unique feature of the analysis allows cracks to appear in the uranium dioxide fuel as it is heated and the growth of the cracks can be traced as a function of linear power generated in the rod. The code can predict such things as pellet deformations and the stress and strain distributions within the pellets and the cladding. The three-dimensionality of the analysis allows a more detailed view of these stresses and strains compared with the usual one-dimensional codes in common use today, and the two-dimensional codes that are also being developed.

Introduction

This paper is devoted to a description of a three-dimensional finite element study of nuclear fuel rods during startup. The objective of a three-dimensional study is to provide additional insight into the stresses and deformations within a fuel rod. It should be noted that there are numerous excellent fuel rod codes in one and two dimensions as will already be apparent from the papers presented at the conference. This paper presents an extension of these efforts to three dimensions in order to provide a means of studying the interaction between axial and plane stress distributions within the fuel.

To understand the objectives of such a three-dimensional model, it is necessary to recapitulate upon a number of observations concerning fuel pellets situated within a cylindrical cladding, as shown in Figure 1. During startup, as heat is uniformly generated within the fuel, the thermal gradient causes stresses in the fuel that are high enough to deform the fuel and crack it, as shown in exaggerated form in Figure 1. If the gap between the fuel and its cladding is small enough, then the pellet can contact the cladding and cause it to deform as shown. The three-dimensional model must be able to trace this process. In addition, it should be versatile enough to permit generalizations as shown in Figure 2. There, the behavior of a fuel rod is traced during a single cycle. In Figure 2, the changes in a fuel section are shown schematically. Cracks grow and may close depending on the fuel temperature and the plastic behavior of the fuel will also change with temperature, as illustrated.

The finite element method is ideally suited to such a study because of its inherent versatility. The region of interest in a fuel rod is shown in Figure 3, which also illustrates how the region is modeled by finite elements.

Nature of Model

The basis for the finite element method of stress analysis used in the three-dimensional model is comprehensively presented by Professor O. C. Zienkiewicz in his book, The Finite Element Method in Engineering Science.[1] In the finite element method, the structure is idealized by being cut into a finite number of elements. In each element, it is assumed that the displacements vary in a simple fashion, the magnitudes depending

on the displacements at the nodes. Nodes are frequently taken at the corners of the element. Computer programs using the finite element method minimize the strain energy expressed in terms of the nodal displacements to obtain a solution. In general, while the inherent error drops to a negligible value as the element size becomes very small, the cost of a computation tends to increase with the number of nodes and the number of elements.

The present paper describes a three-dimensional finite element computer program using an 8-noded box element (Figure 4). This element is used in preference to a tetrahedronal element for three major reasons. First, such an element will ease the burden of input data. Second, the shear error which is commonly introduced by using tetrahedronal elements (particularly when they are fairly large) is reduced. This is done by following a suggestion of R. W. Clough[2]. Nine internal degrees-of-freedom are included in the box element. The net effect is to permit fewer elements to be used in the model. Finally, with the 8-noded box, stresses can be obtained at the middle of each face, thus permitting stresses to be obtained on the surface of the structure.

Information on the isoparametric approach is given in References 3 to 5. These papers describe 3-D elements with more than 8 nodes as well as the 8-noded elements. Elements with more than 8 nodes, though excellent in principle, tend to require much larger amounts of computer time and memory space to set up the element stiffness matrices. In addition, round-off error can be of significant magnitude, particularly in the stress computations. For these reasons, the element used in this paper was considered to be preferable.

The element geometry is shown in Figure 4. The x, y, z coordinates are conventional right-handed rectangular coordinates. The ξ, η, ζ coordinates are the parametric coordinates which will be discussed more fully in a subsequent section where the program logic is presented. Nodes 1, 2, 3, and 4 are in clockwise sequence around the bottom as viewed from the top. (Any side of the box can be considered the top. The numbering can start at any node.) Nodes 5, 6, 7, and 8 are above nodes 1, 2, 3, and 4, respectively as shown in Figure 4.

Program Logic

Figure 4 shows an element with 8 arbitrary nodes as described by Zienkiewicz[1]. A set of skew parametric coordinates (ξ, η, ζ) is set in the element such that the values are either +1 or -1 on the faces. The node numbering is such that nodes 1, 2, 3, and 4 go clockwise around the bottom when viewed through the top and nodes 5, 6, 7, and 8 are above nodes 1, 2, 3, and 4, respectively.

The relationship between the Cartesian (x, y, z) coordinates and the parametric (ξ, η, ζ) coordinates is obtained by defining functions N_1, $N_2 \ldots N_8$ as follows:

$$
\begin{aligned}
N_1 &= (1/8)\ (1-\xi)\ (1-\eta)\ (1-\zeta) \\
N_2 &= (1/8)\ (1-\xi)\ (1+\eta)\ (1-\zeta) \\
N_3 &= (1/8)\ (1+\xi)\ (1+\eta)\ (1-\zeta) \\
&\vdots \\
N_8 &= (1/8)\ (1+\xi)\ (1-\eta)\ (1+\zeta)
\end{aligned}
\qquad (1)
$$

Thus each N function has a value of 1 at its corresponding node and zero at all other nodes. In addition, the N functions vary linearly with ξ, η, ζ. The parametric representation of the Cartesian coordinates is then,

$$
\begin{aligned}
x &= N_1x_1 + N_2x_2 + \ldots N_8x_8 = \{N_n\}^T \{x_n\} \\
y &= N_1y_1 + N_2y_2 + \ldots N_8y_8 = \{N_n\}^T \{y_n\} \\
z &= N_1z_1 + N_2z_2 + \ldots N_8z_8 = \{N_n\}^T \{z_n\}
\end{aligned}
\qquad (2)
$$

in which $\{x_n\}$, $\{y_n\}$, $\{z_n\}$ list the nodal coordinates of the box in sequence.

To provide for transformation of strain derivatives from the (ξ, η, ζ) to the (x, y, z) coordinate system, it is necessary to make use of the Jacobian matrix.

$$
[J] = \begin{bmatrix}
\frac{\partial x}{\partial \xi} & \frac{\partial y}{\partial \xi} & \frac{\partial z}{\partial \xi} \\
\frac{\partial x}{\partial \eta} & \frac{\partial y}{\partial \eta} & \frac{\partial z}{\partial \eta} \\
\frac{\partial x}{\partial \zeta} & \frac{\partial y}{\partial \zeta} & \frac{\partial z}{\partial \zeta}
\end{bmatrix}
\qquad (3)
$$

Substituting eq. (2) into eq. (3) gives,

$$
[J] = \begin{bmatrix}
\frac{\partial N_1}{\partial \xi} & \frac{\partial N_2}{\partial \xi} & \cdots & \frac{\partial N_8}{\partial \xi} \\
\frac{\partial N_1}{\partial \eta} & \frac{\partial N_2}{\partial \eta} & \cdots & \frac{\partial N_8}{\partial \eta} \\
\frac{\partial N_1}{\partial \zeta} & \frac{\partial N_2}{\partial \zeta} & \cdots & \frac{\partial N_8}{\partial \zeta}
\end{bmatrix}
\begin{bmatrix}
x_1 & y_1 & z_1 \\
x_2 & y_2 & z_2 \\
\vdots & \vdots & \vdots \\
x_8 & y_8 & z_8
\end{bmatrix}
\qquad (4)
$$

Eq. (4) permits [J] to be evaluated at any given position once the nodal coordinates are specified. (Normally [J] varies with position in the box element.)

Since Gaussian integration will be used in summing the strain energy in the element, it is important to note that an element of volume in the x, y, z coordinate system is related to the corresponding element of volume in the ξ, η, ζ coordinate system by

$$
dV_{xyz} = |J|\ dV_{\xi\eta\zeta}
\qquad (5)
$$

We can write

$$\frac{\partial N_1}{\partial \xi} = \frac{\partial N_1}{\partial x}\frac{\partial x}{\partial \xi} + \frac{\partial N_1}{\partial y}\frac{\partial y}{\partial \xi} + \frac{\partial N_1}{\partial z}\frac{\partial z}{\partial \xi} \tag{6}$$

and similar relations for the other derivatives. In matrix form, these equations are:

$$\begin{bmatrix} \frac{\partial N_1}{\partial \xi} & \frac{\partial N_1}{\partial \eta} & \frac{\partial N_1}{\partial \zeta} \\ \frac{\partial N_2}{\partial \xi} & \frac{\partial N_2}{\partial \eta} & \frac{\partial N_2}{\partial \zeta} \\ \vdots & \vdots & \vdots \end{bmatrix} = \begin{bmatrix} \frac{\partial N_1}{\partial x} & \frac{\partial N_1}{\partial y} & \frac{\partial N_1}{\partial z} \\ \frac{\partial N_2}{\partial x} & \frac{\partial N_2}{\partial y} & \frac{\partial N_2}{\partial z} \\ \vdots & \vdots & \vdots \end{bmatrix} \begin{bmatrix} \frac{\partial x}{\partial \xi} & \frac{\partial x}{\partial \eta} & \frac{\partial x}{\partial \zeta} \\ \frac{\partial y}{\partial \xi} & \frac{\partial y}{\partial \eta} & \frac{\partial y}{\partial \zeta} \\ \frac{\partial z}{\partial \xi} & \frac{\partial z}{\partial \eta} & \frac{\partial z}{\partial \zeta} \end{bmatrix} \tag{7}$$

The last matrix in eq. (7) is the transpose of [J]. The equality of a matrix equation is preserved if the order of all the terms is reversed and each matrix is transposed. Doing this to eq. (7) and multiplying through by $[J]^{-1}$ gives

$$\begin{bmatrix} \frac{\partial N_1}{\partial x} & \frac{\partial N_2}{\partial x} & \cdots \\ \frac{\partial N_1}{\partial y} & \frac{\partial N_2}{\partial y} & \cdots \\ \frac{\partial N_1}{\partial z} & \frac{\partial N_2}{\partial z} & \cdots \end{bmatrix} = [J]^{-1} \begin{bmatrix} \frac{\partial N_1}{\partial \xi} & \frac{\partial N_2}{\partial \xi} & \cdots \\ \frac{\partial N_1}{\partial \eta} & \frac{\partial N_2}{\partial \eta} & \cdots \\ \frac{\partial N_1}{\partial \zeta} & \frac{\partial N_2}{\partial \zeta} & \cdots \end{bmatrix} \tag{8}$$

In eq. (1), we define eight N functions. For describing the displacements in the box we will use these functions and three additional ones,

$$\begin{aligned} N_9 &= 1 - \xi^2 \\ N_{10} &= 1 - \eta^2 \\ N_{11} &= 1 - \zeta^2 \end{aligned} \tag{9}$$

We will specify that the displacements u, v, w in the x, y, z directions are given by equations similar to eq. (2).

$$\begin{aligned} u &= N_1u_1 + N_2u_2 + \ldots N_{11}u_{11} = \{N_n\}^T \{u_n\} \\ v &= N_1v_1 + N_2v_2 + \ldots N_{11}v_{11} = \{N_n\}^T \{v_n\} \\ w &= N_1w_1 + N_2w_2 + \ldots N_{11}w_{11} = \{N_n\}^T \{w_n\} \end{aligned} \tag{10}$$

where u_n, v_n, w_n, for n = 1 to 8 are nodal displacements while for n = 9, 10, 11, they are internal degrees-of-freedom whose values will be chosen to minimize the element

strain energy.

The strains are given by

$$\varepsilon_x = \frac{\partial u}{\partial x}, \quad \varepsilon_y = \frac{\partial v}{\partial y}, \quad \varepsilon_z = \frac{\partial w}{\partial z}$$

$$\gamma_{xy} = \frac{\partial u}{\partial y} + \frac{\partial v}{\partial x} \tag{11}$$

$$\gamma_{yz} = \frac{\partial v}{\partial z} + \frac{\partial w}{\partial y}$$

$$\gamma_{zx} = \frac{\partial w}{\partial x} + \frac{\partial u}{\partial z}$$

Substituting eq. (10) into eq. (11) gives

$$\begin{Bmatrix} \varepsilon_x \\ \varepsilon_y \\ \varepsilon_z \\ \gamma_{xy} \\ \gamma_{yz} \\ \gamma_{zx} \end{Bmatrix} = \begin{bmatrix} \frac{\partial N_1}{\partial x} & 0 & 0 & \frac{\partial N_2}{\partial x} & 0 & 0 & \cdots & \frac{\partial N_{11}}{\partial x} & 0 & 0 \\ 0 & \frac{\partial N_1}{\partial y} & 0 & 0 & \frac{\partial N_2}{\partial y} & 0 & \cdots & 0 & \frac{\partial N_{11}}{\partial y} & 0 \\ 0 & 0 & \frac{\partial N_1}{\partial z} & 0 & 0 & \frac{\partial N_2}{\partial z} & \cdots & 0 & 0 & \frac{\partial N_{11}}{\partial z} \\ \frac{\partial N_1}{\partial y} & \frac{\partial N_1}{\partial x} & 0 & \frac{\partial N_2}{\partial y} & \frac{\partial N_2}{\partial x} & 0 & \cdots & \frac{\partial N_{11}}{\partial y} & \frac{\partial N_{11}}{\partial x} & 0 \\ 0 & \frac{\partial N_1}{\partial z} & \frac{\partial N_1}{\partial y} & 0 & \frac{\partial N_2}{\partial z} & \frac{\partial N_2}{\partial y} & \cdots & 0 & \frac{\partial N_{11}}{\partial z} & \frac{\partial N_{11}}{\partial y} \\ \frac{\partial N_1}{\partial z} & 0 & \frac{\partial N_1}{\partial x} & \frac{\partial N_2}{\partial z} & 0 & \frac{\partial N_2}{\partial x} & \cdots & \frac{\partial N_{11}}{\partial z} & 0 & \frac{\partial N_{11}}{\partial x} \end{bmatrix} \begin{Bmatrix} u_1 \\ v_1 \\ w_1 \\ u_2 \\ v_2 \\ w_2 \\ \vdots \\ u_{11} \\ v_{11} \\ w_{11} \end{Bmatrix} \tag{12}$$

The matrix in eq. (12) is readily obtained from that in eq. (8). In the program it is suitably multiplied by the material stiffness matrix to obtain stress and the strain energy per unit volume matrix.

The strain energy in this element varies with position in the element. To perform the integration, use is made of a 2-point Gaussian numerical integration. In this approach, it is necessary to evaluate the strain energy at the 8 points for which ξ, η, ζ have values of ± 0.57735026. It is evident that a key matrix in this approach is that on the right in eq. (8). The strain energy is minimized with respect to the 9 internal degrees-of-freedom thus giving their values in terms of the 24 external degrees-of-freedom. Using these relations, the strain energy and stress matrices are provided in terms of the external degrees-of-freedom only.

Before concluding this discussion of the 8-noded isoparametric element, it should be mentioned that a variety of other 3-D elements have been recommended from time to time (see References 3 to 5). Some of these elements were tried in the process

of developing this program. An element with 27 nodes was found to give difficulty both from round-off error in the stress computation and from long running time. The present 8-noded element with 9 internal degrees-of-freedom was recommended by Clough[2]. The gain by use of the 9 internal degrees-of-freedom is at the expense of not exactly satisfying compatibility between nodes. This disadvantage is not present when a tetrahedron element is used. It can be shown that as the 8-noded box element is reduced in size, the "compatibility" error drops to zero, so a convergent process is being used. It can be shown by numerical experimentation that the 8-noded box element can in fact be quite large without introducing errors at all comparable to the shear error present when tetrahedron elements are used.

Geometric Input Data

The bulk of the input data consists of coordinates of nodal points, element nodal numbers, load conditions, and boundary conditions.

In locating nodes and elements, the following procedure is followed:

(a) The three-dimensional solid is divided by a number of nonintersecting surfaces. (Much like slicing a loaf of bread.) The surfaces need not be flat or parallel though they frequently are.

(b) Each such surface is further subdivided by a number of nonintersecting lines. (Much like the lines on a piece of paper.) The lines need not be straight or parallel though they frequently are.

(c) Each such line is further subdivided into a number of divisions to give the nodal points. Nodal points are numbered in sequence along each line, line by line, and surface by surface.

(d) The nodes on each surface are said to belong to the same partition. Partitions are numbered in sequence from one side of the solid to the other. (The first partition contains the first nodal points.)

(e) The number of divisions in adjacent lines can vary to provide for grading of the mesh.

(f) 8-noded box elements are formed between adjacent surfaces. They are numbered sequentially between each pair of adjacent surfaces. The numbering continues for successive adjacent surfaces in turn going from one side to the other of the solid structure. (Although in theory the boxes need not be square, it is recommended that they be as square as the shape of the structure permits.) The first element has nodes in the first partition.

For the application to a fuel rod consisting of cylindrical fuel pellets inside a cylindrical cladding, an example of a division into elements is shown in Figure 5. There, a segment of the fuel which is formed by the surfaces of two adjacent radial cracks in the UO_2 is modeled. In this drawing, there are 96 nodes within the upper half of the fuel pellet wedge (symmetry is assumed here), and 114 nodes within the cladding. More nodes are used within the cladding to provide detailed stress calculations there.

Model Implementation

In order to implement the finite element computer program described above, an average temperature profile is computed for the pellet and cladding. The final distortions and crack configurations are calculated by an iterative process such that a state of stress equilibrium is reached. At first, calculations are made on an uncracked pellet. The surface hoop stresses are found to be very high -- above the UO_2 fracture strength. The pellet is then divided into a number of wedges. (16 wedges were used to begin with.) A new calculation of stress showed that the hoop stress at the mid-width of the wedge surface was now well below the UO_2 fracture stress, indicating that too many wedges had been chosen. Thus, the calculation was repeated with only eight wedges. This time, the maximum wedge hoop stress was near the fracture stress, indicating that the correct number of wedges had been chosen. Similar iterative processes were followed (at the same time) to generate axial cracks. It was also found, on the basis of a static fracture criterion, that a central region within the UO_2 pellet did not crack. It remained whole. In addition, the interaction between the clad and the fuel was followed by inserting mathematical springs between finite-element nodes on the clad and in the UO_2. The axial forces due to adjacent pellets was also modeled in the same manner. Springs model the interaction between the tension in the clad and the axial compression in the central region of the pellet, as shown in Figure 6. Springs restrain the circumferential motion of the uncracked surfaces of the wedge.

The deformation of the hot central portion of the fuel was found to be such that it was necessary to introduce plasticity effects. The plastic behavior of the fuel was modeled by using a secant modulus in the thermo-elastic computer program.

Use of Three-Dimensional Code

The computer program can be used to follow the startup deformations, strains, and stresses in a nuclear fuel rod. To illustrate this capability, a UO_2 pellet within a cladding of Zircaloy was studied. Some typical observations on the results are made below, for a moment in time during the startup ramp. In order to study a situation when the pellet would contact the cladding, a very small initial gap was assumed between the fuel and cladding. The material properties used for the UO_2 fuel and Zircaloy cladding were drawn from various sources in the open literature.

In Figure 7 we show the deformations of the pellet and clad. There are a number of points to notice. First, the pellet is cracked into eight wedge-like portions. A central region reaching about half way along the pellet radius remains uncracked. There is a transverse crack around the waist of the pellet that extends inwards until an area of compressive stress is reached. Second, each wedge is bowed outwards. At the pellet axis on the top and bottom, the wedges have expanded axially due to thermal expansion, and are pushing on the adjacent pellets. The upper edges of the pellet are in

contact with the cladding, which now exhibits deformation due to the contact pressure of the pellet. We note that for this startup configuration (when pellet creep effects have not yet come into prominence), the cladding does not touch the waist of the pellet. Contact is only made near the pellet ends.

The distribution of axial and hoop stresses that occur in the central plane of one wedge are shown in Figures 8 and 9, respectively. A region of high compressive stress occurs in the wedge interior, and on the outer portions, there are tensile stresses that reach the tensile fracture stress in magnitude. (More heating would, therefore, produce another transverse crack at about two-thirds the pellet height.) Near the existing transverse crack, the axial stresses are low, having been relieved by the presence of the crack. The pellet hoop stresses are compressive within the central uncracked portion, and also within the interior of the wedge. The tensile hoop stresses increase towards the exterior of the pellet. At the top edge, which is in contact with the clad, the tensile hoop stress is a maximum. There, it is near to the tensile fracture stress of UO_2, and this is the position where a new radial crack would initiate upon further heating to form a new wedge. The details of the stress distribution will, of course, vary with the design details of the pellet itself.

The stresses in the clad are interesting because they exhibit areas of both tensile and compressive stress. The clad hoop stress is tensile near the pellet-pellet interface, due to the pellet clad contact. But towards the waist of the pellet, where there is no contact yet, the hoop stress becomes slightly compressive. Similarly, the clad axial stress is compressive in the very local region of the pellet-clad contact point. There is also a slight compressive axial stress near the pellet waist at the exterior clad surface. This view of the stresses illustrates that within both the pellet and the clad, there exists a rather complicated stress distribution.

Conclusing Remarks

An approach to the three-dimensional study of the behavior of nuclear fuel rods during startup has been outlined. By means of this approach, the localized behavior of the fuel rod can be followed during startup. Further developments are in progress, particularly in the area of fuel creep behavior, which becomes important during the later stages of fuel rod life.

References

[1] ZIENKIEWICZ, O. C., The Finite Element Method in Engineering Science, McGraw-Hill, London (1971).

[2] CLOUGH, R. W., personal communication, April 1971.

[3] CLOUGH, R. W., "Comparison of Three-Dimensional Finite Elements," (Keynote address in Symposium on Application of Finite Element Methods in Civil Engineering - Edited by W. H. Rowan and H. M. Hackett), American Society of Civil Engineering, 1970.

[4] IRONS, B. M., "Engineering Applications of Numerical Integration in Stiffness Methods," AIAA Journal, 4, 2035-2037 (1966).

[5] ZIENKIEWICZ, O. C., IRONS, B. M., ERGATOUDIS, J., AHMAD, S., and SCOTT, F. C., "Isoparametric and Associated Element Families for Two and Three Dimensional Analysis," Proc. Course on Finite Element Methods in Stress Analysis, TAPIR, Tech. Univ. of Norway, Trondheim, 1969.

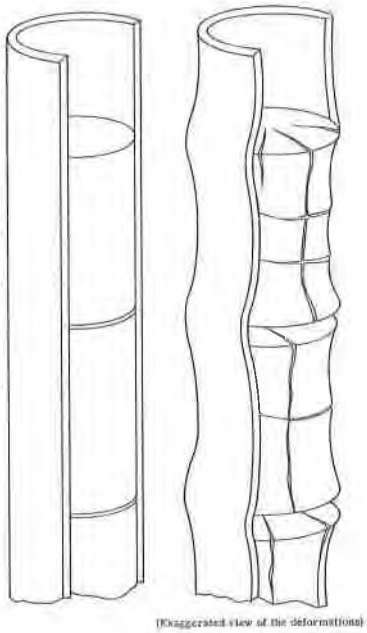

Fig. 1 **Fuel Rod Before and After Startup**

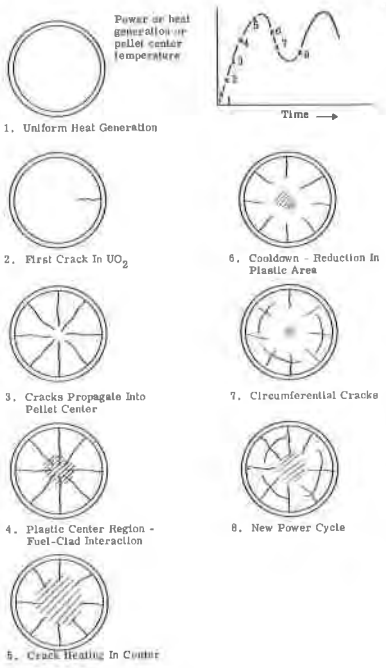

Fig. 2 **Pellet Behavior Model**

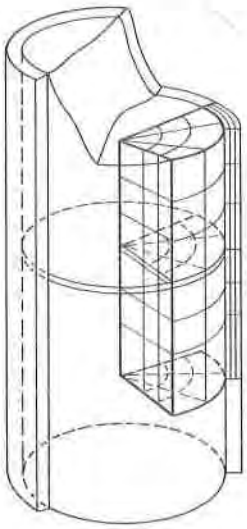

ig. 3 **Finite Element Idealization of Fuel Rod**

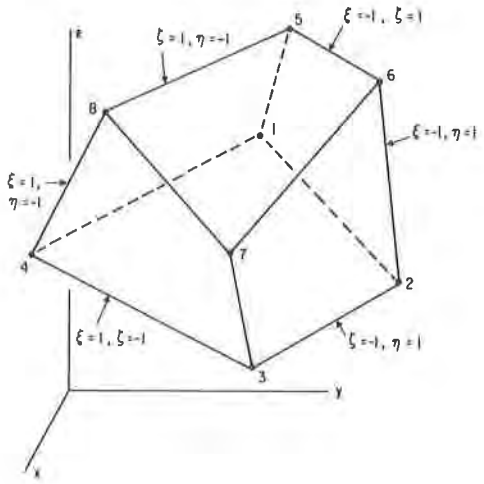

Fig. 4 Element with 8-Nodes Showing Rectangular and Parametric Coordinate Systems

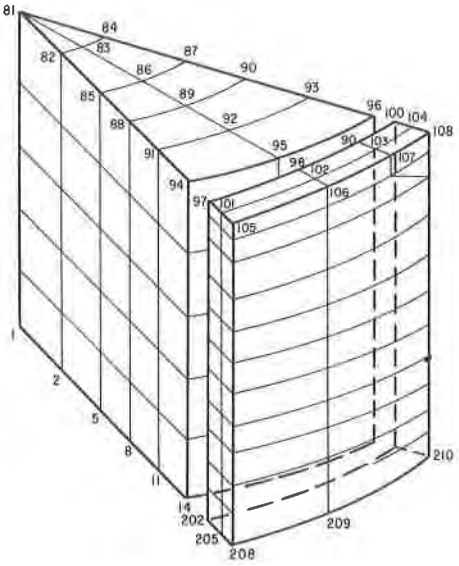

Fig. 5 Nodal Arrangement in the Fuel and Cladding

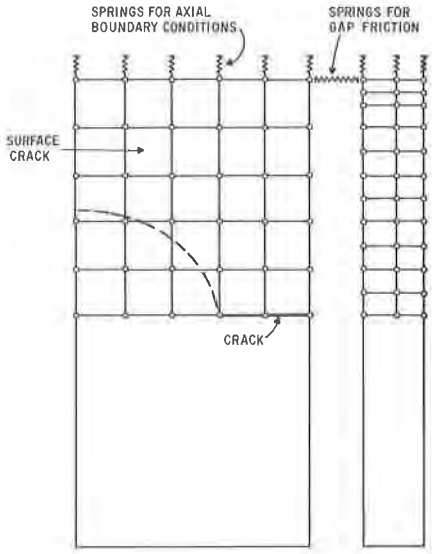

Fig. 6 Introduction of Springs to Simulate Boundary Conditions

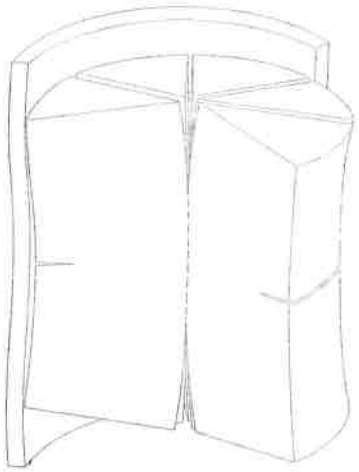

Fig. 7 Deformations in a Fuel Rod During Startup

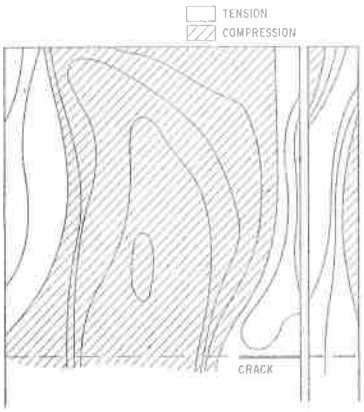

Fig. 8 Axial Stress in the Central Plane of a Pellet Wedge

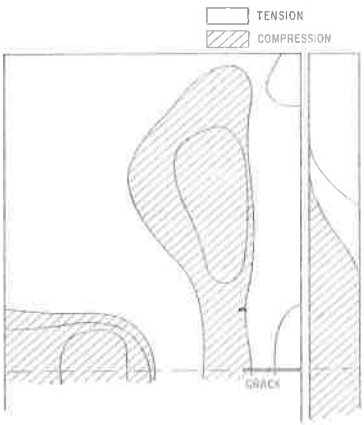

Fig. 9 Hoop Stress in the Central Plane of a Pellet Wedge